Experimental Techniques
https://doi.org/10.1007/s40799-022-00559-4

RESEARCH PAPER

Experimental Dynamic Characterization of Rigid-Flex PCB Systems

J. Bell[1] · L. Redmond[2] · K. Carpenter[3] · J. P. de la Croix[4]

Received: 24 May 2021 / Accepted: 19 February 2022

Abstract
Rigid-flex printed circuit boards (PCBs) are used in many applications that range from mobile electronic devices to low-volume medical tools. Dynamic characterization of a rigid-flex system is difficult because the system exhibits large deformation in the joints, panel-to-panel contact, and other sources of dynamic nonlinearities and complexities not present in traditional PCBs. To date, rigorous test methods for the dynamic characterization of rigid-flex PCB systems have not been proposed. The objective of this paper is to present a case study of a rigid-flex PCB system from the NASA Jet Propulsion Laboratory (JPL), demonstrating nonlinear characterization and a modal testing protocol that sufficiently characterizes the frequencies, mode shapes, damping, and nonlinear properties of the structure. Additionally, single panels and a rigid-flex assembly without aluminum components are tested to draw more generalized conclusions regarding appropriate test protocols for other rigid-flex systems. The nonlinear characterization of the rigid-flex structures was performed using the test for homogeneity, an examination of energy-dependent resonance and damping, and the use of the Hilbert transform. Based on the results of this study, it is recommended to first use the Hilbert transform to efficiently identify the presence of a nonlinearity then investigate energy-dependent frequency characteristics and nonlinear damping, which are likely to be influenced by the rigid-flex system's geometry. All of the rigid-flex systems exhibited energy-dependent frequency characteristics and damping nonlinearities that increased with increased range of motion of the PCB panels about the Nomex hinges and increased with an increase in the number of hinges activated in a particular mode. However, the addition of the aluminum reinforcing components reduced both forms of nonlinearity. To enable modal testing of the rigid-flex structure with aluminum components, it was necessary to understand the resonance replicability and the sensitivity to suspension and excitation orientation to separate noise from local and global resonances.

Keywords Modal testing · Dynamic characterization · Rigid-flex PCB · Robotics · Nonlinear dynamics

Introduction

As demand increases for electronic device functionality, considerations for mobility, volume, and mass are at the forefront of circuit board design. Rigid-flex printed circuit board (PCB) components, a structure with rigid PCB sections with flexible connecting components, allow for new design possibilities and more compact devices by permitting increased mobility, reducing the amount of wiring in the system, and eliminating the need for connectors [1]. Rigid-flex circuits are particularly useful in aerospace applications as mass and volume considerations often drive design. In some cases, switching from traditional to rigid-flex circuitry can reduce the mass of the circuit system by up to 90% [2].

Dynamic characterization of rigid-flex PCB systems via modal testing is a difficult task. The connection between individual PCB panels and flexible hinges results in

✉ J. Bell
jsb6@clemson.edu

[1] Glenn Department of Civil Engineering, Clemson University, South Palmetto Blvd, Clemson, SC 29631, USA

[2] Glenn Department of Civil Engineering and Department of Mechanical Engineering, Clemson University, South Palmetto Blvd, Clemson, SC 29631, USA

[3] NASA Jet Propulsion Laboratory, Robotic Vehicles and Manipulators Group, 4800 Oak Grove Dr, Pasadena, CA 91109, USA

[4] NASA Jet Propulsion Laboratory, Robotic Systems Estimation, Decision, and Control Group, 4800 Oak Grove Dr, Pasadena, CA 91109, USA

Published online: 01 March 2022

nonuniform wave propagation and exhibits damping effects, that are not found in a single-component system. While work has been performed on studying the dynamics of traditional PCB [3–5], there is a lack of guidance in the literature for dynamic characterization via modal testing of rigid-flex circuit board systems. The objective of this paper is to present a case study of a rigid-flex PCB system from NASA Jet Propulsion Laboratory (JPL), demonstrating nonlinear characterization and a modal testing protocol that sufficiently characterizes the frequencies, mode shapes, damping, and nonlinear properties of the structure. Additionally, single panels and a rigid-flex assembly without aluminum components are tested to draw more generalized conclusions regarding appropriate test protocols for other rigid-flex systems. In this paper, a variety of methods for dynamically characterizing the nonlinearities present in rigid-flex systems are examined using NASA JPL's rigid-flex PCB robot, PUFFER (Pop Up Folding Flat Explorer Robot). PUFFER is an origami robot that utilizes PCB as the structural system connected by Nomex hinges and flex circuitry [6]. In addition, single PCB panels with and without Nomex hinges, and a PUFFER without aluminum support structure are considered For each test method examined, additional discussion is provided regarding best practices, data interpretation, and any challenges or benefits observed in testing. This paper aims to provide a methodology for (1) detecting the source of the nonlinearity (local/global phenomena and physical cause), (2) identifying the form of the nonlinearity (geometric, material, etc.), and (3) quantifying the relationship between the nonlinearity and relevant modal testing system inputs (magnitude of excitation, frequency range, etc.) in PUFFER and provide generalization to other rigid-flex PCB systems. Finally, recommendations for appropriate modal testing procedures of rigid-flex PCB systems are presented based on the nonlinearities identified using the aforementioned methodology.

Literature Review

Modal testing on solid PCB panels is often performed with a shaker and involves an iterative procedure of updating material and geometric assumptions. Solid PCBs typically behave linearly and can be approximated by analytic solutions available for vibrations of plates. Arabi et al. [3] outlines a process of dynamically validating a model using orthotopically elastic material properties obtained through testing. Bell et al. [7] has outlined that for the case study robot PUFFER, isotropic elastic properties are sufficient. Several other studies have been conducted on the dynamic performance of mounted components on a populated PCB sample [1, 5, 8, 9].

The dynamic characterization of rigid-flex PCB has not been performed extensively; however, modal testing of nonlinear structures has been studied by many researchers. A common approach is to assume that linear assumptions are sufficient for a dynamic assessment [10]. A superior modal test for a flexible structure considers the assumptions made about the linearity of the system in traditional testing methods, boundary conditions, and excitation ranges [11]. For example, limiting the excitation frequency bandwidth was imperative during modal testing on a robotic manipulator [12], where the frequency range was restricted from the system's nonlinear response zone. Other case studies of modal testing of flexible structures use procedures tailored for the specimen under analysis [13]. Additionally, the form of the nonlinearity influences test complexity and propensity for error. For example, plate structures with anisotropic material properties [14] have an inherently simpler test approach than structures with weak nonlinearities due to joint friction [15]. The most appropriate testing procedures tend to be specific to the system geometry and the level of rigor necessary for satisfactory results. A well-explored approach in strongly nonlinear systems is quasi-static modal analysis (QSMA), which resolves the force–displacement behavior of individual modes [16]. For the rigid-flex PCB system explored in this paper and systems of similar complexity (comparable assembly and level of flexibility), the dynamic behavior can be quantified using traditional modal testing methods.

The most typical types of nonlinearities expected are geometric, inertial, material, and damping. Nomenclature varies between authors as nonlinearities from boundary conditions are sometimes categorized as a geometric nonlinearity [17] or as a separate entity [18]; this paper adopts the latter approach. For flexible systems, the strength of geometric nonlinearities is expected to change with varying degrees of flexibility. Inertial nonlinearities compliment geometric nonlinearities by quantifying the velocity and inertial properties associated with large displacements. Material nonlinearities are not expected for a rigid-flex system, as the materials do not exhibit a nonlinear stress–strain relationship that are the typically cause of dynamic nonlinearities [19]. However, nonlinear damping, such as hysteretic damping [20] should be considered a strong possibility in rigid-flex PCB systems.

Case Study Structure: PUFFER

The case study structure PUFFER is a small rover designed for planetary exploration that is optimized for volume and mass reduction [6]. It is composed of several sections: the rigid-flex body (assembled and disassembled in Fig. 1), an aluminum cover on top and aluminum base, wheels, and an antenna. PUFFER's rigid-flex PCB is composed of

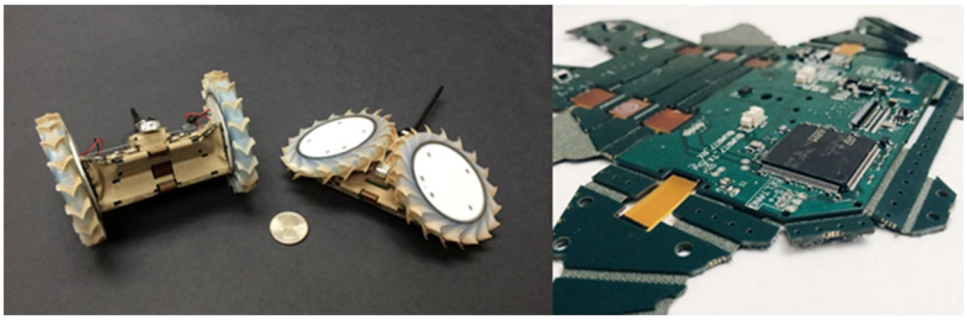

Fig. 1 Assembled in Unfolded and Folded Configurations (left) [21] and Disassembled (right) PUFFER Rigid-Flex PCB

traditional FR4 panels (with six 1 mil thick copper layers) connected by a Nomex fabric backing and flex circuitry. The Nomex is applied to the PCB with an acrylic bond. For testing, the chassis is examined by removing the wheels, antenna, and mounted hardware. This chassis is tightly assembled and has eleven 1.7 mm wide Nomex joints. Two variants of the chassis are tested; the chassis with and without aluminum components. The mass of the flight-like (aluminum components included) chassis is 0.151 kg. PUFFER can fold to reduce its volume by approximately 65%, enabling it to move under obstacles and store compactly.

FEM to Inform Modal Testing

To inform the setup of the various dynamic tests examined in this paper, an initial FEM of PUFFER was constructed. Component-level modal tests were used to inform material properties of the FEM [7]. A benchmark [3] was used to test the influence of orthotropic elastic material properties on the dynamics of the PCB panel. It was found that the maximum change in first three resonant frequencies of a solid PCB panel was only 4.3% when an equivalent effective isotropic elastic modulus was used. Thus for simplicity, the initial model used isotropic properties. For a flexible system, the dynamic response is largely controlled by the properties of the joints with minimal bending of the PCB panels, thus the isotropic-orthotropic change has an even smaller impact on an assembled rigid-flex structure. The Nomex joints were modeled as plate elements with reduced bending stiffness as outlined in [7], and the material and damping properties are given in Table 1. Note that material parameters with a prime designation have been tailored using the following methodology. The equations for bending and axial rigidity of the Nomex plate elements are provided in Eqs. 1 and 2, respectively.

$$B_r = \frac{E' t'^3}{12(1-\nu)} \tag{1}$$

$$A_r = \frac{E' t'}{(1-\nu^2)} \tag{2}$$

Table 1 Initial FEM Material and Damping Properties for Solid PCB and Nomex Hinges [7]

	Property	Value
PCB	E	$25.5GPa$
	ρ	2.08275E-06 kg · mm^{-3}
	ν	0.18
	α	10.698 ms^{-1}
	β	0 ms
Nomex	E'	25.5GPa
	ρ'	2.07E-06 kg · mm^{3}
	ν	0.36
	α	1.177E-05 ms^{-1}
	β	8.86E-05 ms
	δ	2.25
	t'	0.237 mm

α and β refer to the mass-proportional and stiffness-proportional components of Rayleigh damping, respectively.

To reduce the flexural stiffness of the plate elements by a flexural stiffness reduction factor, say δ, the following adjustments are made:

$$E' = E\sqrt{\delta} \tag{3}$$

$$t' = \frac{t}{\sqrt{\delta}} \tag{4}$$

$$\rho' = \rho\sqrt{\delta} \tag{5}$$

Note that the identical elastic modulus values for the PCB and Nomex are merely coincidental and were identified through component modal testing and model correlation.

Nonlinear Characterization for Informed Modal Testing

This section focuses primarily on the flight-like variant of PUFFER's chassis. It is expected that the flight-like rigid-flex PCB system exhibits nonlinearities that originate from several sources. The first source of nonlinearity comes from the large difference in stiffness of the rigid and flexible sections of the system. Additionally, rigid-flex PCB systems can exhibit isolated component motion, local vibrations, nonuniform wave propagation, and a hysteretic response. Lastly, dynamic complexities are introduced at the hinges due to the damping in the Nomex fabric. This section includes an overview of the test program to characterize nonlinearities in rigid-flex PCB, a description of the methods applied, and the observed results.

Overview of Test Program to Characterize PCB Nonlinearities

In this section, nonlinearities are examined through modal methods. In order to detect the presence of nonlinearities, it is first assumed that the flight-like system has of weak or avoidable nonlinearities and traditional modal methods may be applied [22]. The results of the test program to characterize nonlinearities validate if the assumption is true. The panels of flight-like PUFFER are expected to exhibit relatively small displacements at resonance with various suspension configurations. This was preliminarily checked with the initial FEM by extracting displacements at resonance and was ensured by beginning modal testing with low levels of excitation. However, if a full rigid-flex system manifests strong unavoidable nonlinearity or modal bifurcations generate additional nonlinear resonances, a new theoretical framework needs to be applied [18].

To examine the nonlinearities present in the individual Nomex joints, two test specimens with dimensions of 152.4 mm × 152.4 mm × 1.212 mm were used. The first is a solid PCB panel and the second test specimen is a rigid-flex PCB panel with a Nomex hinge in the center (as shown in Fig. 2). Several tests to identify nonlinearities in the Nomex joint are presented, including tests for homogeneity, tests for energy-dependent frequencies and damping, and the use of the Hilbert Transform. These tests are repeated for PUFFER's rigid-flex system with no aluminum components attached to draw more generalized conclusions about the dynamic behavior of rigid-flex PCB systems. Finally, the nonlinearities present in a flight-like configuration of PUFFER with aluminum components were characterized using the same tests. The selection of appropriate boundary conditions and excitation points was performed prior to modal testing of the flight-like configuration of PUFFER and is discussed in Section 5.

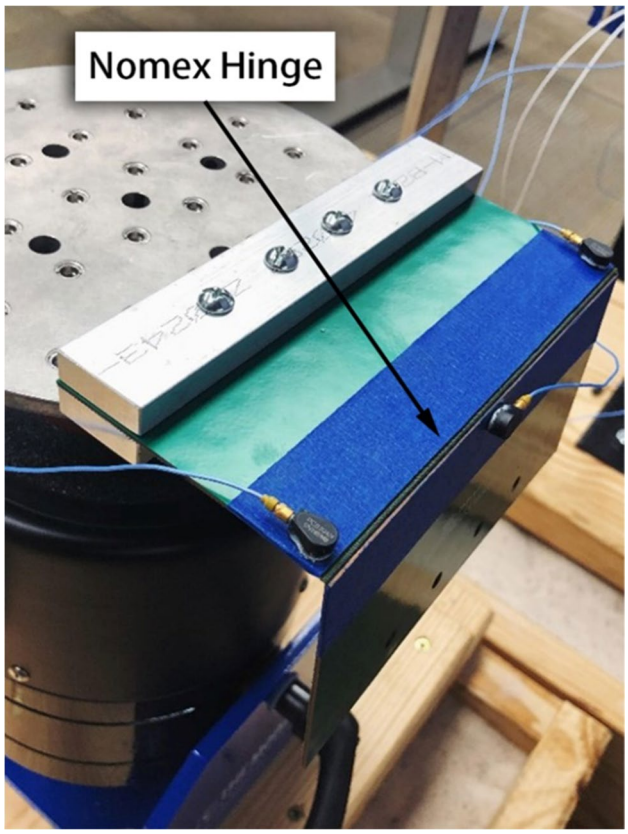

Fig. 2 Cantilevered Hinged Rigid-Flex Sample

For the hinged panel sample, modal testing was performed using The Modal Shop K2075E040 electrodynamic shaker with an expander head. The test specimens were attached to the expander head by being directly fixed to the head through the bolt holes pictured. It was found that the impact of the nonlinearity is a function of the joint bend radius. For this reason, the tests were performed with a hinged PCB sample cantilevered on the shaker expander head, as shown in Fig. 2. A random excitation with a flatline PSD ranging from 0–4500 Hz was used for testing (magnitude varied by test). The accelerometers used were ceramic ICP uniaxial sensors (0.8gm) with sensitivities of 100 ± 1 mV/g secured with Loctite 451. The FRFs are constructed with a Hanning window, 30 averages, and 33% overlap. In some cases, the sample rate was adjusted between for a finer frequency resolution, with a spacing of 0.1 Hz, to accurately determine energy-dependent modal parameter curves. The modal tests performed for PUFFER's rigid-flex system without the aluminum components and with aluminum components was performed using a random vibration excitation with varying levels of flatline input acceleration between 0.05 and 1.0 g^2/Hz. An image

of PUFFER's suspended rigid-flex system without the aluminum components is shown in Fig. 3.

For rigid-flex PCB systems, a common geometric nonlinearity exists that is dependent on joint radius. Figure 2 shows a cantilevered rigid-flex PCB panel with a central Nomex hinge. For modes with large mass participation in the plane orthogonal to the span of the PCB as shown, the geometric nonlinearity operates similarly to a simple pendulum [18]. For the PUFFER rigid-flex system without aluminum components the nonlinearities will be shown to amplify. However, in the flight-like PUFFER rigid-flex system with aluminum components, the range of motion of the panels is limited and panels often have boundary conditions on multiple edges, yielding a weaker nonlinearity and enabling traditional modal testing as discussed in Section 5.

As the flight-like PUFFER rigid-flex PCB system with the aluminum components exhibits only weak nonlinearities, an investigation into nonlinear normal modes (NNMs) [23] is not considered. Only identification of the functional form of the nonlinearity is analyzed. The objective of the nonlinear characterization is to use traditional modal methods to (1) detect the source of the nonlinearity (local/global phenomena and physical cause) and (2) identify the form of the nonlinearity (geometric, material, etc.), (3) quantify the relationship between the nonlinearity and relevant system inputs (magnitude of excitation, frequency range, etc.).

Methodologies for Identifying and Characterizing Nonlinearities

The following modal testing and analysis procedures were performed to detect the presence and the type of nonlinearity in rigid-flex PCB systems: the (1) test for homogeneity, (2) application of the Hilbert transform on FRF data, (3) test for energy-dependent resonance, and (4) analysis of damping nonlinearities. These tests are conducted at both the panel and system level to develop recommendations for testing a wide range of rigid-flex PCB systems.

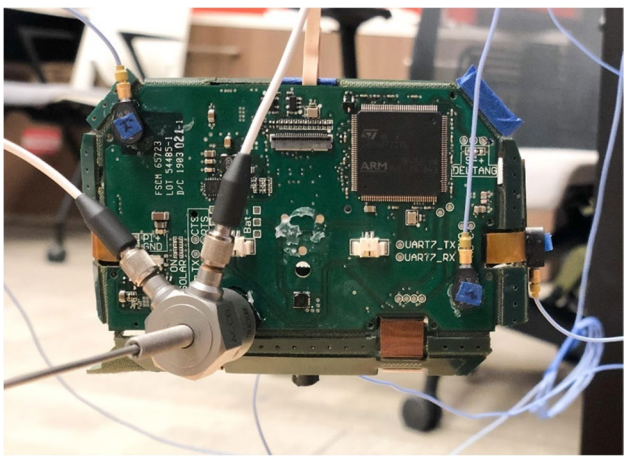

Fig. 3 PUFFER's Rigid-Flex System without Aluminum Components

Test for Homogeneity

A key component of a linear system is that the test specimen holds homogeneity, which is a restricted form of the principle of superposition. Given the responses y_1, y_2 of a system due to the input forces x_1, x_2, respectively, the principle of superposition states that the following holds for linear systems:

$$\psi x_1(t) + \eta x_2(t) = \psi y_1(t) + \eta y_2(t),\ \psi, \eta \in \mathbb{R} \tag{6}$$

The principle is violated if the quantities are not equal. Homogeneity is a weaker and restricted form of superposition because the second response factor, η, is set to 0.

$$\psi x_1(t) = \psi y_1(t) \forall \psi \tag{7}$$

If this principle holds true, the system FRF effectively is independent of input signal magnitude and is indicative of but does not guarantee a linear system.

Use of the Hilbert Transform on FRF Data

The Hilbert transform, a linear operator, is commonly used for nonlinear detection in the frequency domain [24–26]. The Hilbert transform of a function $f(x)$ is given by Eq. (8),

$$H\{f(x)\} = \frac{1}{\pi}\int_{-\infty}^{\infty} \frac{f(a)}{x-a} da \tag{8}$$

and this is a particularly useful operation when applied to a general complex analytic function, $G(z)$. If z is a complex variable, Cauchy's formula can be used:

$$G(z) = \frac{1}{2\pi i}\oint \frac{G(\lambda)}{\lambda - z} d\lambda \tag{9}$$

assuming that $G(z)$ is a transfer function, it can be expressed in the frequency domain by

$$G(\omega) = \sum_{r=1}^{m} \frac{i\omega X_r}{\omega_r^2\left(1 + i\delta_r\right) - \omega^2} \tag{10}$$

because $z \in \mathbb{C}$, z can be generally written in complex terms, $z = \omega + i\epsilon$. If the series is multiplied out to produce the ratio of two polynomials, it becomes:

$$G(z) = izA\frac{\left(z-a_1\right)\left(z-a_2\right)\cdots\left(z-a_{2m-2}\right)}{\left(z-b_1\right)\left(z-b_2\right)\cdots\left(z-b_{2m}\right)} \tag{11}$$

where A is a constant, a_n are the zeros of the function, and b_n are the poles. When the zeros and poles are plotted in the complex plane, the surface integral can be evaluated through

contour integration. Performing this, the line integral along the real axis is expressed by:

$$G(\omega_c) = -\frac{1}{\pi i} PV \int_{-\infty}^{\infty} \frac{G(\omega)}{\omega - \omega_e} d\omega \tag{12}$$

where the quantity PV denotes that the Cauchy Principal Value of the integral has been taken. Because (12) takes the form of the Hilbert transform (8), the Hilbert transform of the transfer function may be taken (13).

$$H\{G(\omega_c)\} = H(\omega_c) = -\frac{1}{\pi i} PV \int_{-\infty}^{\infty} \frac{G(\omega)}{\omega - \omega_e} d\omega \tag{13}$$

The above expression can then be further subdivided into the real and imaginary parts, (14) and (15), respectively.

$$H_r\{G(\omega_c)\} = H(\omega_c) = -\frac{1}{\pi i} PV \int_{-\infty}^{\infty} \frac{im(G(\omega))}{\omega - \omega_e} d\omega \tag{14}$$

$$H_i\{G(\omega_c)\} = H(\omega_c) = -\frac{1}{\pi i} PV \int_{-\infty}^{\infty} \frac{re(G(\omega))}{\omega - \omega_e} d\omega \tag{15}$$

where $H_r \in \mathbb{R}$, $H_i \in \mathbb{I}$. In the case of a general system, which need not be linear, the transfer function is more specifically the FRF, which is the relationship of the Fourier transforms of the output and input signals, respectively.

$$G(\omega) = \frac{\mathcal{F}\{y(t)\}}{\mathcal{F}\{x(t)\}} = H_r(\omega) + iH_i(\omega) \tag{16}$$

The Hilbert transform can be used in nonlinear detection by applying the transformation to the FRF. Because it is a linear operator, for arbitrary frequency-domain functions m, n, it effectively holds the following constraint [27]:

$$\forall \zeta, \kappa \in \mathbb{R}, H\{\zeta m(\omega) + \kappa n(\omega)\} = \zeta H\{m(\omega)\} + \kappa H\{n(\omega)\} \tag{17}$$

A Hilbert transformation on a linear system yields the original FRF [24]. Distortions between the pre and post transformed FRF data sets can be attributed to the presence of nonlinear effects. Determination of specific nonlinear characteristics, not just the presence of nonlinearities, can be informed by the Hilbert transform [28], but this is impractical for the purpose of a general analysis methodology. A simple Hilbert transformation in the frequency domain is a powerful tool in assessing the presence of a nonlinearity and identifying nonlinear ranges.

Energy-Resonant Frequency Relationship

A common visual indicator of a nonlinearity is an energy-dependent shift in resonant frequency [18, 29]. Energy-dependent resonant frequencies can be checked by examining the FRF peaks at varying degrees of input acceleration, most commonly a flatline random PSD. Frequency-energy backbone curves can then be constructed, indicating the impact of the nonlinearity on resonant linear modes.

Testing for Damping Nonlinearities

Another common and expected form of nonlinearity is a damping nonlinearity [30] that can often be neglected for weak nonlinearities [31]. In practice, equivalent viscous damping or a hysteretic damping approach [20, 32] is often applied to capture more complex damping dynamics. Assessing the damping nonlinearities present in a rigid-flex system and the sources determines if the effects need to be considered for accurate modal analysis. In this study, damping is calculated using the half-power bandwidth (HPB) method, that assumes sufficiently spaced modes and linear properties. The stronger the presence of a nonlinearity, the more inaccurate the estimated damping from HPB will be. Torvik [33] illustrates that a reduction in estimating error is obtained by choosing a larger bandwidth than that conventionally used (*i.e.*$\eta \neq 1/\sqrt{2}$, where $\eta = 1.0$ is at the peak response) and presents a ratio of equations to assess damping with a strongly linear amplitude-value relationship in strongly nonlinear systems.

Because of the absence of strong nonlinearities, the authors have determined that a correction to the half-power bandwidth calculation is not required for rigid-flex PCB systems similar in PCB layup and construction to the case study structure (see Section 3).

Results from Characterization of Nonlinearities Through the Proposed Methods

The test for homogeneity was checked by comparing the magnitude of frequency response functions of modal tests with varying input magnitudes for the rigid-flex PCB panel with a Nomex hinge and the PUFFER rigid-flex system with and without aluminum components. Limited by output force and the weight of the expander head, all tests were conducted with flatline PSD values beginning at 0.05 g^2/Hz and ending at 1.0 g^2/Hz, with 0.05 g^2/Hz increments. In all cases, the FRF magnitude exhibited a linear change between varying degrees of input force, and the homogeneity criterion holds, but does not prove linearity through the frequency range examined (0–4500 Hz).

To provide a second test for the presence of nonlinearity, the Hilbert transform is performed on sets of FRF data. To visually illustrate the effects of the Hilbert transform, the FRF plots of two different panel tests, a solid PCB and the cantilevered, hinged PCB, are compared. The Hilbert transform was also computed for the PUFFER rigid-flex system without aluminum components and the flight-like configuration of PUFFER with aluminum components. In

all cases, the transformation was performed in MATLAB by computing the analytic signal through a fast Fourier Transform (FFT) FFT and inverse FFT (IFFT) procedure [34]. It should be noted that this procedure encounters the same truncation errors typically observed in a FFT process. To minimize truncation errors, the FRF data is normalized [28] by the following transformation. For a frequency response function $f \in FRF$:

$$f \rightarrow [0, 1] \tag{18}$$

$$||H(\omega)|| = 1 \tag{19}$$

where $||H(\omega)||$ is the Euclidean norm of the Hilbert-transformed FRF data. The results of the pre and post Hilbert-transformed FRFs for a solid (linear) PCB specimen and the hinged (nonlinear) piece, from 100–1500 Hz (frequency range in which both specimens exhibit several resonances), is shown in Fig. 4, although the analysis can be conducted on both the real and imaginary components of the FRF [35].

Figure 4 provides a visual illustration of the Hilbert transform on both linear and nonlinear systems over a full frequency spectrum. Both the real and imaginary parts of the functions exhibit a similar pattern. It is apparent that the solid PCB panel has a Hilbert transform that agrees well with the original FRF, where the Hilbert transform of the hinged PCB panel deviates from the original FRF significantly. The high deviation between the original and transformed FRF plots of the hinged sample at early frequencies are attributed to inertial response at low excitation frequencies. The Hilbert transform is often used to characterize nonlinearity strength within a neighborhood of a single mode; however, the full frequency range of the panel samples display the effects clearly. The full FRF spectra of PUFFER (shown later in Fig. 10) contains more noise, causing the Hilbert transform plot to be visually less demonstrative of the technique for nonlinear identification. For this reason, a numerical value is often used as an indicator of nonlinear presence and strength.

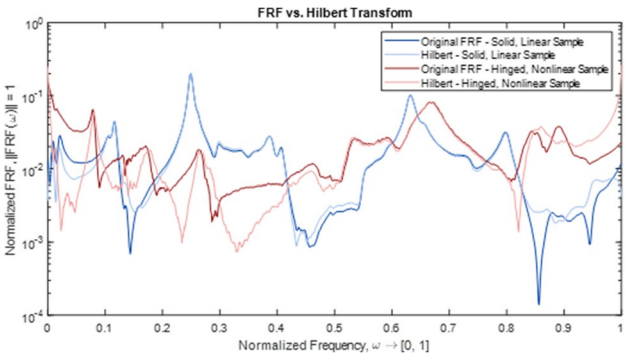

Fig. 4 Original and Hilbert-Transformed FRF of Two PCB Samples

To assess the strength of the nonlinearity, a nonlinear identifier (NLI) is determined, as presented in [28, 36], which utilizes the cross-correlation coefficient. The cross-correlation can be evaluated over specific frequency regions or within proximity to a single vibration mode. The cross-correlation between the original FRF (G) and its Hilbert transform (H), and the NLI, is defined as:

$$R_{GH}(\Delta\omega) = \int_{-\infty}^{\infty} G(\omega)H(\omega + \Delta\omega)d\omega \tag{20}$$

$$NLI = 1 - \left|\left|R_{GH}(0)\right|\right|^2,\ NLI \in [0, 1] \tag{21}$$

The nonlinear index is evaluated at a zero-frequency lag between two selected frequency values, $[\omega_{min}, \omega_{max}] \subset [-\infty, \infty]$. By the index's definition, it is sensitive to geometric nonlinearities that manifest by shifting resonances or introducing nonlinear normal modes, and therefore is an appropriate metric to apply to rigid-flex systems. The NLI may be applied to various resonances to assess the degree of nonlinearity present at or near the resonance, but for simplicity, ± 20 Hz of the first resonant frequency for all cases was analyzed. The zero-lag cross correlation coefficient is also dependent on sample size, so the sampling settings and frequency resolution from all compared data sets are identical. The NLI values are shown below, in Table 2, that illustrate a near order of magnitude increase in NLI from the linear solid sample to the single hinge sample, and nearly twice the NLI for the assembled PUFFER rigid flex system without aluminum components as compared to a single hinge. Once the aluminum components are added, the NLI for the first mode drops to a value closer to the hinged PCB panel, suggesting a weaker and more avoidable nonlinearity.

Next, the possibility of energy-dependent resonant frequencies was investigated. The first three modes of the solid and hinged PCB panels were compared with flatline white noise excitation levels ranging from 0.05 g^2/Hz to 1.00 g^2/Hz in 0.05 g^2/Hz increments. In the FRF data, an increase in noise was observed for higher frequencies (above ~ 3000 Hz), causing the peak separations to be unclear. As expected, there was no change in the resonant frequencies of the solid PCB sample due to changing

Table 2 Nonlinear Indices for Test Specimens

Test Specimen	NLI
Solid PCB Panel	0.0456
Hinged PCB Panel	0.2191
PUFFER rigid-flex system with aluminum components	0.2677
PUFFER rigid-flex system without aluminum components	0.3908

excitation levels using a frequency resolution of 0.25 Hz. For the hinged PCB panel, the maximum resonance shift observed was 0.5 Hz at the third mode, concluding that an individual rigid-flex panel does not exhibit strong energy-frequency dependency. The PUFFER rigid-flex system with and without aluminum components was also excited using a flatline white noise excitation level ranging from 0.05 g^2/Hz to 1.00 g^2/Hz in 0.05 g^2/Hz increments. The PUFFER rigid-flex system without aluminum components had a maximum frequency shift of 3.10 Hz for frequencies between 1000 and 2000 Hz, illustrating a higher degree of nonlinearity with increased system complexity. PUFFER's chassis contains 11 Nomex hinges connecting 6 discrete panels. It is expected that other rigid-flex PCB systems behave similarly, with increased energy-dependency of the system frequencies as the number of joints and discrete PCB panels increases. The FRF plots for PUFFER's flight-like configuration subjected to a flatline 0.1 g^2/Hz excitation level (blue), and a flatline 1.0 g^2/Hz excitation level (red) are shown in Fig. 5, and these excitation values are selected to illustrate the sensitivity to excitation magnitude. Both plots were taken from the same accelerometer on the largest PCB panel on which the aluminum cover is fixed. To construct the FRF, the input frequency ranged from 100–4500 Hz and a Hanning window with 30 averages was applied. The suspension configuration yielding the results in Fig. 5 is not the final tested configuration but one in which PUFFER is suspended near the wheel attachment points. This configuration is selected to maximize the effect of the nonlinearity and to provide an example of excitation sensitivity. In the figure, the y-axis is the transfer function magnitude in log scale, and the x-axis is the frequency in hertz. The most apparent discrepancy is seen between 1000–2000 Hz, a region that the test configuration yielded higher geometric nonlinearities. For the flight-like PUFFER in its final configuration, the resonant frequencies examined and shown in Fig. 10 for model correlation yielded a maximum frequency shift of 2.25 Hz. Thus, the aluminum components helped to decrease the energy dependency of the frequencies from the maximum shift of 3.10 Hz without aluminum components. Another key observation is that there exists a relationship between the strength of the nonlinearity at resonance and the associated modal shape. In all cases where the nonlinearity was the strongest, the displacement at resonance included a significant portion of the primary (top) panel mass rotating about at least one Nomex hinge.

To examine the effects of damping nonlinearities, energy-damping curves were constructed for the cantilevered, hinged PCB panel and the PUFFER rigid-flex system with and without aluminum components leveraging the data from the energy-frequency study. The results of the solid PCB panel had a maximum $\Delta\xi = 0.28\%$ over the range of flatline excitation magnitudes from 0.05 g^2/Hz to 1.0 g^2/Hz. For the hinged PCB sample, the mode selected to calculate the damping was one that exhibited bending about the flexible axis. For the same range of input excitation, the hinged panel exhibited damping values from 0.48% to 1.37%, resulting in a total $\Delta\xi = 0.89\%$ Similar levels of damping variance were not present in modes with displacements characterized by PCB bending, indicating that the nonlinearity was manifest in the flexible joint. Furthermore, damping nonlinearity is magnified by an increased bend in the Nomex hinge. When the hinged PCB sample was tested with both ends fixed and the Nomex hinge lying flat rather than cantilevered with one end free-hanging, the damping was within $\pm 0.25\%$ of a solid PCB panel placed under the same boundary conditions and varying excitation levels. The PUFFER rigid-flex system without aluminum components expectedly exhibited higher levels of nonlinear damping. With the same testing methodology applied, the first mode exhibited damping values between 3.64% and 4.84% for maximum $\Delta\xi = 1.20\%$. To compare simple and complex rigid-flex systems, the damping values from the first mode of both the hinged PCB sample and the rigid-flex system without aluminum components are plotted in Fig. 6 and logarithmic curves are fit to the damping data. The change in damping is a direct result of the increase in the complexity and assembly of the structure. Some of the variance between data points can be attributed to frequency resolution and half power bandwidth calculation approximations, whereas the geometric nonlinearity of the panel's "swinging" motion is anticipated to further increase the overall variation between data points, introducing a level of stochasticity to the system.

This was also observed in the tests of the flight-like PUFFER, where the first mode exhibited damping values

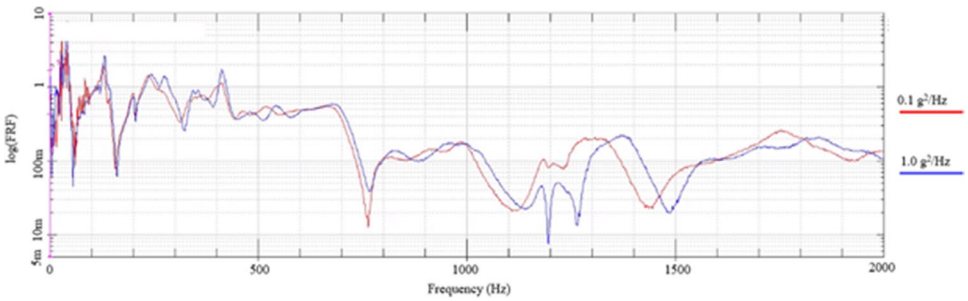

Fig. 5 Plot of Frequency Response Functions of Flight-Like PUFFER's chassis with Varying Excitation Levels

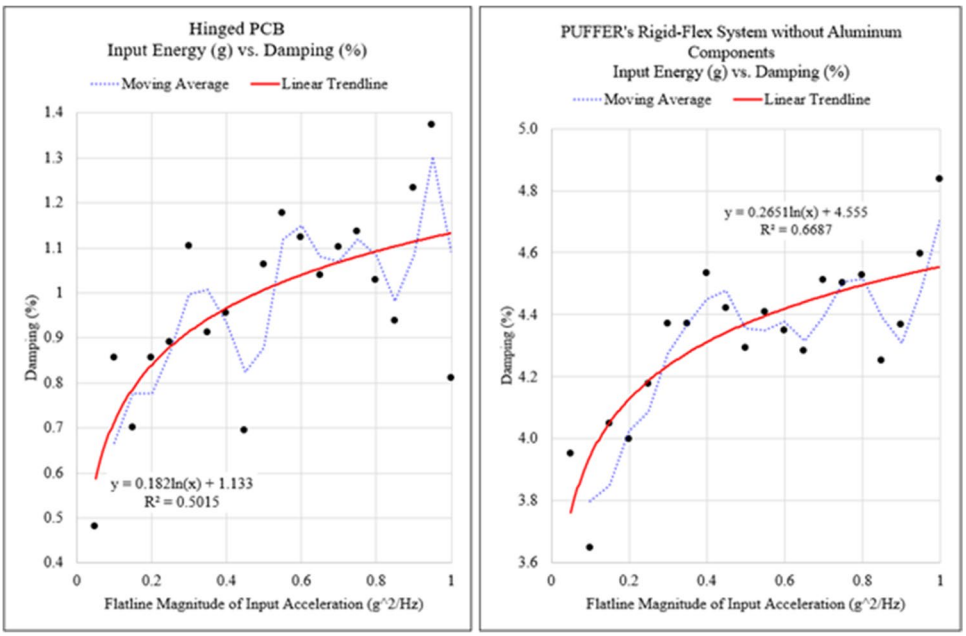

Fig. 6 Logarithmic Curve Fit for Observed Damping Values in the First Model of a Single Hinged Panel and Complex Rigid-Flex System

between 2.25% and 3.05% for maximum $\Delta\xi = 0.9\%$ which is significantly less than the first mode of PUFFER without the aluminum components. For a torsional mode of PUFFER in which motion was limited to a single side of the hinged panel exhibited a very low variation in damping, $\Delta\xi = 0.24\%$. Very high-frequency modes (4000 Hz to 4500 Hz) that exhibited hinge motion showed high variation in damping, up to 6.25%. However, the maximum variation in damping in the first several modes used for model correlation is 0.90%, and this is deemed as acceptable with reference to the rigid-flex system without aluminum components.

Application to Modal Testing

This section has outlined various forms of nonlinearities that are likely to be present in any rigid-flex system. These forms of nonlinearities include energy-dependent frequency characteristics and damping nonlinearities that have increasing influence depending on the geometry of the system. The larger the range of motion of the PCB panels about the Nomex hinges and the more hinges activated in a particular mode, the greater magnitude of nonlinearities due to energy-dependent frequencies. Additionally, larger bend radii for the Nomex hinges results in increased damping nonlinearities. It was also observed that the addition of the aluminum components reduced the energy-dependency of the frequency response and the nonlinear damping of the system. It is recommended to first use the Hilbert transform to efficiently identify the presence of a nonlinearity. Once the presence of a significant nonlinearity is identified, it is recommended that test engineers investigate energy-dependent frequency characteristics and nonlinear damping, which are likely to be influenced by the rigid-flex system's geometry. In addition to these nonlinearities, other complexities must be considered when modal testing rigid-flex PCB systems.

Modal Testing Techniques

This section highlights some unique considerations for modal testing of rigid-flex PCB structures executed on the case study structure, a flight-like configuration of PUFFER with the aluminum components. Such considerations include the boundary conditions and accelerometer placement, excitation magnitude and type, and techniques for capturing localized rigid-body dynamics. The considerations may be applied to similar reinforced rigid-flex structures with weak nonlinearities. All modal testing was performed with the same shaker and accelerometers outlined in Section 3. All test details are specified with the presentation of the results, but a typical approach applied a Hanning window, no cut-off filtering, and a 33% overlap. In this study, modal testing was performed on the flight-like configuration of PUFFER with a free-suspended boundary condition. As mentioned previously, the half-power bandwidth method for damping estimation was used to calculate the damping. Alternative methods of estimating damping for higher values of damping are presented in [37] and the authors compared the half-power results to the proposed method and saw negligible differences. Based on the results of many modal tests, the authors of this paper recommend (1) constructing boundary conditions such that the effects of geometric nonlinearities are weakened as much as possible, (2) performing sensitivity studies at varying degrees of excitation amplitude (as

covered in Section 4), excitation type and location, and (3) examining the panel responses individually prior to assessing a full system modal response. Details of each of these recommendations are presented in the following sections.

Accelerometer Placement and Boundary Conditions

Determining the most appropriate sensor location for modal testing has been widely researched, with techniques ranging from effective impedance [38] to hierarchal approaches with modal kinetic energy as a quantifier [39]. For rigid-flex systems, the authors recommend performing the following outlined procedure based on preliminary FEM results.

To select the best initial points of accelerometer attachment, the initial modal FEM was used to calculate the optimum driving point (ODP) and the average driving point residue (ADPR), as outlined in [40]. The ODP is an expression of the overall modal motion across a span of relevant frequencies of a test subject, and for a point j and a mode r, with normalized modal displacement ϕ, is defined by:

$$ODP(j) = \prod_{r} |\phi_{rj}| \tag{22}$$

The ADPR gives a quantitative description of the relationship between overall modal motion with respect to the resonant frequency. For frequencies ω, the ADPR is calculated by:

$$ADPR(j) = \sum_{r} \frac{\phi_{rj}^2}{\omega_r^2} \tag{23}$$

These operations reveal the areas with proportionally large amounts of modal motion, which serve best as initial accelerometer placement locations. For the uniaxial accelerometers, the modal displacements were calculated as normal to the plane defined by the rigid PCB panels.

The final consideration for accelerometer placement is to select the appropriate type and number of accelerometers to minimize accelerometer mass and excess wiring. For a single-hinged, cantilevered rigid-flex PCB sample (Fig. 2), with the accelerometer mass placed on the free-hanging panel, a sensitivity study was performed on the effects of added mass on FEM frequencies and are presented in Table 3.

The most accurate model correlations are possible when the added weight of the accelerometers is relatively low. For this reason, the authors recommend keeping the added weight of instrumentation as less than or equal to 10% of the mass participation of the components contributing to expected resonances. For PUFFER with the aluminum components, this was less than ~ 12 gm, and the modal testing leveraged five accelerometers totaling 4.0 gm.

Suspension effects on modal test results have historically been a cause for concern. Traditionally, a metric for the adequacy of the suspension system is a comparison of the relative stiffnesses between the test subject and the suspension system [41]. When stiffness is subsequently introduced by a suspension system, the rigid body frequencies have nonzero values that would ideally be significantly distanced from the first elastic mode of the structure. In a study on an automotive system, Wolf [42] concluded that the minimization of suspension effects is achieved when the suspension system is attached to the most massive part of the test subject and the rigid body modes occur at frequencies below one-tenth the frequency of the first elastic mode. Flexible structures often exhibit very low-frequency modes due to flexible joints, making it more difficult to select an appropriate suspension system. In addition, suspension systems have the potential to restrict or change the motion of the rigid-flex PCB structure and induce additional damping and unwanted geometric nonlinearities at resonance. For PUFFER with the aluminum components attached, the suspension system consisted of pre-stretched elastic bands to reduce the impact of the suspension system on the frequencies that were attached using Loctite 454. Figure 7 shows the ideal suspension setup for the flight-like PUFFER's chassis. This orientation is specifically useful as it places the massive aluminum cover at the bottom, minimizing any potential inertial effects at resonance. The band attached directly to the aluminum serviced primarily as a stabilizer to allow the stinger to be perpendicular to the aluminum base. The recommended process for determining the suspension points and appropriate suspension system is summarized below.

First, the ODP and ADPR can be used to determine the non-optimum points on the structure, the areas that exhibit relatively low modal motion over the relevant frequency range. The reduction in motion considerably reduces suspension bouncing and subsequently minimizes additional stiffness and damping that is artificially introduced. Next, the cables attached to the frame structure should be analyzed to ensure that the resonant frequencies are far from the test specimen's elastic frequencies. After, an initial FEM can be used to verify the maximum expected displacement of the system is small. For PUFFER with the aluminum components attached, an initial FEM was created using generated

Table 3 Impact of Lumped Masses on Resonant Frequency

Mass Added (gm)	% Change in Fundamental Frequency from Baseline Model
1.6	0.3
2.4	0.42
3.2	0.59
6.0	1.10
12.0	3.22

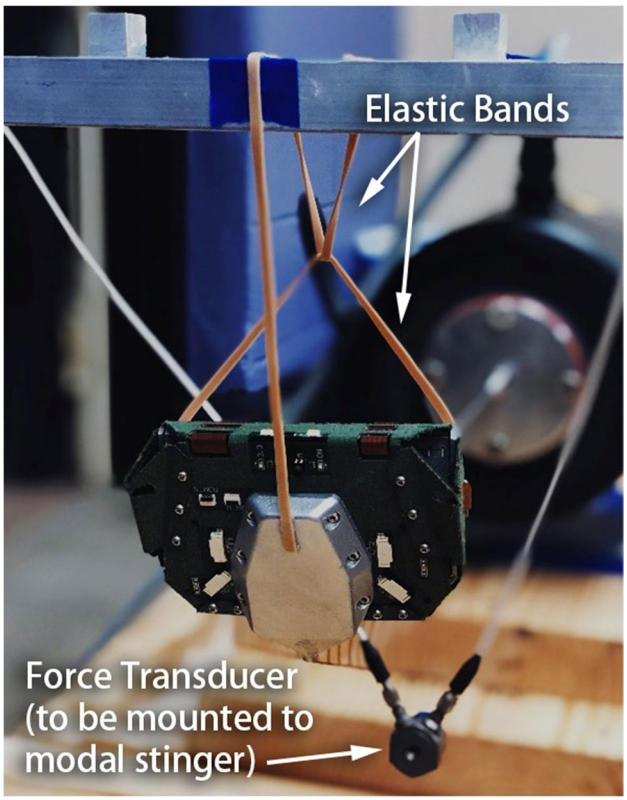

Fig. 7 PUFFER's Suspension System

random acceleration time history data with the same target PSD as the test procedure. The mean response (g) of the flight-like configuration of PUFFER at the attachment points was then extracted from model results, multiplied by a factor of three, and applied to the elastic bands. It was found that the strain in the bands from subjecting them to three times the modal acceleration of the flight-like PUFFER were sufficiently low.

After, consideration should be given to the attachment points for the suspension system to ensure they allowed for complete folding of the rigid-flex PCB, and they prevent the addition of stiffness to the Nomex joints by the suspension system. For the flight-like configuration of PUFFER, the ideal attachment points were two elastic bands in the rear attached to the aluminum base – the most massive part of the rigid-flex system – and one elastic band attached to the front aluminum cover. The front elastic band was extremely loose and was in place only to keep the chassis level during resonance to prevent off-axis excitation and stinger bending effects. These attachment points were determined by examining the sensitivities of the vibrations of the panel with respect to input force at various connection points. The modal parameters extracted from this configuration were also obtained through similar suspension orientations. As the magnitude of the random signal applied was increased, an off-axis orientation resulted in higher levels of stochastic panel vibration. Additionally, other attempted configurations restricted the motion of the free panels and affected the FRF results.

Finally, the impact of the suspension system on the structural damping and resonant frequencies should be evaluated. For PUFFER with the aluminum components attached, this was done by suspending the rigid-flex body in the test orientation with elastic bands that varied in stiffness by a factor of 3, and the results were compared. The shift from pre-stretched softest bands to stiffest bands manifested as negligible shifts in the FRF plots, giving confidence in minimizing the effects of the suspension stiffness.

Excitation

Based on results of tests on the flight-like configuration of PUFFER, it is recommended that modal tests use either a random vibration or a sufficiently fast sine sweep as determined by initial sensitivity studies. The excitation types considered for the flight-like PUFFER testing were limited to a random vibration and a sine sweep as they are the most standard and accessible. All runs included accelerometer dB overload safeguards in the event of a larger than expected resonant response. It was observed that a fast sine sweep or random input signal yielded more satisfactory data than a slower sweep. This change is attributed to a slower sine sweep developing residual motion within the rigid-flex system, resulting in messy FRF data. This was benchmarked with sine sweeps of rates of 100 Hz change (blue) / min and 4 Hz change (red) / min. as shown in Fig. 8.

In addition to the excitation type, the excitation orientation must be considered for rigid-flex PCB systems. It is recommended that if an initial FEM is available, a comparison of the modal mass participation over the relevant frequency range be conducted and the excitation placed on the largely contributing sections. For the flight-like configurations of PUFFER, attaching the stinger to a massive portion (for PUFFER, the aluminum base) yielded more accelerometer agreement between accelerometers at the predicted resonances than alternative attachment points. Alternative attachment points yielded poor data due to the magnification of geometric nonlinearities and local accelerations by a significant increase in mass at those locations. Additionally, the excitation applied to smaller panels dramatically altered the resulting FRF data, particularly at higher frequencies. This phenomenon is shown in Fig. 9; where two FRF data sets were obtained with identical accelerometer configurations and sampling settings but with the stinger on the aluminum base or a side panel. In the figure, each colored line represents an accelerometer data set corresponding to the same color dot on the PUFFER shown in Fig. 9. Finally, it was determined that attaching the stinger to the most massive

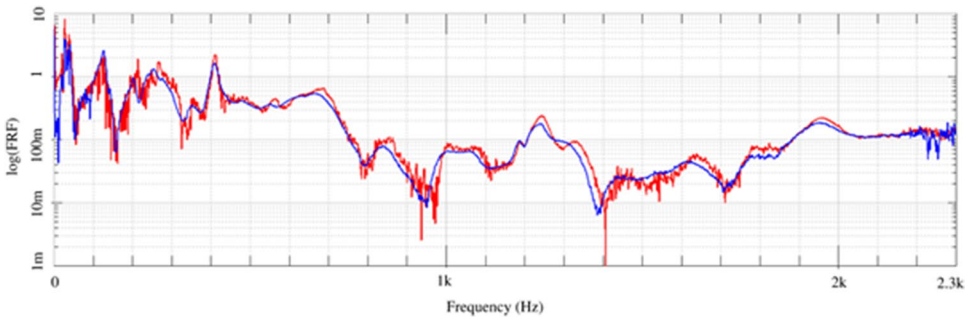

Fig. 8 Fast (100 Hz/min in blue) vs. Slow (4 Hz/min in red) Sine Sweep FRF Results

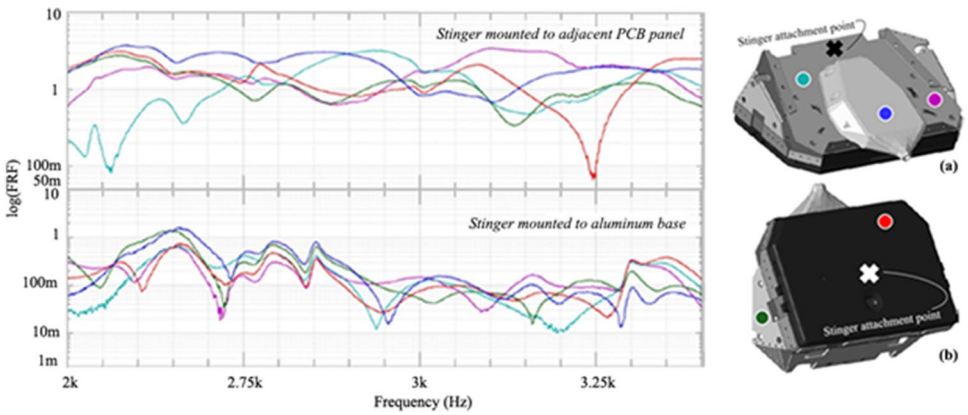

Fig. 9 Sine Sweep from 2000–3800 Hz with Varying Stinger Attachment Locations for Multiple Accelerometer Locations

portion yielded the most consistent results for capturing the targeted modes. This was validated by checking 8 different stinger attachment points and performing the same modal testing protocol with each input location and analyzing the consistency and replicability of the resulting data. The lack of any response consistency between the two shown FRF data sets illustrates the importance of attachment location for rigid-flex systems.

Techniques for Capturing Panel Rigid Body Dynamics

Rigid-flex systems allow for isolated resonances and asymmetric response because of the "loose" connectedness of the panels that comprise the structure. This section analyzes the local resonances and presents testing methodologies to examine these phenomena.

The nature of a rigid-flex PCB system permits sections to dynamically behave independently, and a rigid-flex panel may or may not allow for uniform wave propagation, resulting in varying levels of response from different panels. It is recommended that some roving of accelerometers is conducted during testing to understand if some of the detected frequencies are propagation of local panel modes through the system. During testing, PUFFER with the aluminum components attached, exhibited a resonance from some suspension and excitation orientations that was absent from others. This peak, located at ~ 930 Hz, was evident only when both the stinger and the accelerometers were attached to the aluminum base. The aluminum base is made of two aluminum sections that clasp around a large PCB panel that is housed for protection. To further investigate suspicions of a local phenomenon causing the 930 Hz response, a more detailed breakout model of the aluminum base and the housed PCB panel was created. This model confirmed that there existed a "drumming" mode of the internal PCB panel predicted to be at 932 Hz. Since localized dynamics were identified on part of the flight-like configuration of PUFFER, additional testing was performed focusing on each of the panels that largely contributed to the dynamic response under isolated analysis to check for anomalies and discrepancies. This was performed by acquiring acceleration data from the specific portion of the system and the neighborhood of panels adjacent to it. Local resonances can be found by identifying frequencies only present when examining certain panels that are substantiated by accelerometers on neighboring panels. Accelerometers on varying parts of the test structure, in the case of a local resonance, will show a wide spread of FRF data with no correlation.

Modal Test of Rigid-Flex PCB System (PUFFER) with Aluminum Components

The final test of the flight-like configuration of PUFFER was performed using a random excitation from 100 – 4500 Hz, a standard Hanning window, 25 averages, and a sampling rate

that meets the Nyquist criterion. The final orientation was a free-suspended condition with the stinger placed on the aluminum base, the most massive portion of the flight-like PUFFER. Accelerometers were populated on the aluminum base, aluminum head, and the neighboring PCB panels (to detect localized panel motion) in accordance with the optimum placement determined from pretests. The mode shapes of the aluminum pieces were primarily used for visual model correlation, and it was ensured that the rest of the structure agreed with the predicted mode shape. The plot of all six accelerometer FRF measurements is plotted in Fig. 10, with frequency in Hz on the x-axis and a log scale FRF value for the y axis.

Highlighted in yellow, the lower-frequency resonances have been shown to be inconsistent and present because of the stochastic rigid-body motion of the panels at the lower frequencies. This was observed under nearly all testing conditions and was verified by placing two uniaxial accelerometers on various panels and examining the differences in the acceleration responses between the pairs. In most cases, it was apparent that a rigid body panel response was occurring. The four modes used for model correlation accounted for 88% mass participation in the FEM and are circled in red. Highlighted in green, small resonances following the second mode under analysis are prominent in the set but are inconsistent between data sets. For a modal correlation, these are neglected, as these resonances indicate the effects of a hysteretic response, or a local resonance activated by the specific excitation orientation. Additionally, these frequencies were not predicted by the FEM. Highlighted in pink, higher frequency data consistently resulted in more complex, uncapturable modes due to increased mode shape complexity and higher levels of stochastic behavior. Highlighted in black is the frequency range exceeding the designated frequency cutoff. Table 4 shows the results of the initial FEM, the testing results, and the percent difference.

It is important to note that the authors used multiple runs with varying suspension configurations that allowed for the full motion of specific modes to infer the analysis of a single set of FRF data. For example, the flight like PUFFER's first resonance mimics a "breathing" motion, where the chassis expands and contracts at resonance. It was ensured that the boundary conditions did not place any geometric restriction on this motion by attaching the suspension to a panel active at resonance. Understanding the resonance replicability and the sensitivity to suspension and excitation orientation was critical in separating noise from local and global resonances. When applicable, phase shift diagrams were used to ensure true modal resonance was achieved at the relevant frequencies, and in all cases, the mode shapes and coherence plots were examined.

Table 4 Flight-Like PUFFER Modal Test Correlation Results

Mode No	FEM Resonant Frequency (Hz)	Testing Resonant Frequency (Hz)	% Difference
1	586.97	612.00	4.26%
2	1056.90	998.00	5.57%
3	1385.50	1300.00	6.17%
4	1438.30	1433.00	0.37%

Conclusions

This paper has proposed the first rigorous test protocol for the dynamic characterization of the rigid-flex PCB system PUFFER and has provided insights to suggest appropriate test procedures for other rigid-flex PCB systems. To sufficiently characterize the nonlinear properties of rigid-flex PCB systems, it is recommended that the test engineer first verify presence of a nonlinearity using the Hilbert Transform. Second, a preliminary study on the impacts of energy-dependent frequencies and nonlinear damping is recommended using the presented methods. It can be expected that a rigid-flex system, at the very least, exhibits weak geometric nonlinearities that need to be considered. The results of this study suggest that individual rigid-flex panels do not exhibit strong energy-frequency dependencies and this effect can largely be neglected in a FEM and still achieve a satisfactory modal correlation. Third, a study on boundary conditions and dynamic response is recommended to ensure the resulting modal test data represents the true system response. Individuals performing modal tests on rigid-flex

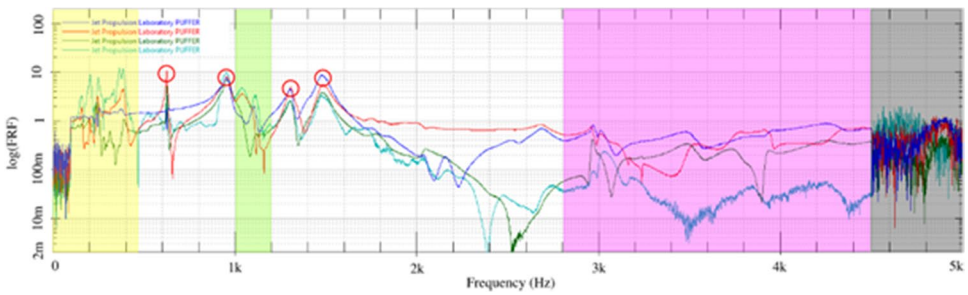

Fig. 10 Final FRF Data Set from Flight-Like PUFFER Modal Test

systems should structure the test such that the excitation point is at a relatively massive portion of the test structure, and roving data should be collected from the neighborhood of panels to identify a consistent FRF response at expected modes. Stinger and accelerometer location are instrumental in the acquisition of useable data, and sensitivity studies on FRF results should be performed on the test structure prior to final data collection. Fourth, sensitivity to excitation type and magnitude should be examined. This study found the system response to a sine sweep excitation was highly dependent on sweep rate and slow sweep rates resulted in poor FRFs due to residual motion within the rigid-flex system. Finally, any local rigid-flex panel resonances should be identified in modal testing via roving of accelerometer and excitation locations.

Authors' contributions Not applicable.

Funding This work was supported by the NASA South Carolina Space Grant Consortium, grant project numbers 521383-RP-CM002 (REAP) and 521193-CM001 (GRF). The research was carried out with the Jet Propulsion Laboratory, California Institute of Technology, under a contract with the National Aeronautics and Space Administration (80NM0018D0004).

Data availability Not available.

Code availability Not applicable.

Declarations

Conflicts of Interest Not applicable.

References

1. Rapala-Virtanen T, Jokela T (2005) New materials and build-up constructions for advanced rigid-flex PCB applications. Circuit World 31(4):21–24
2. Isaac J (2007) Rigid-flex technology: mainstream use but more complex designs. CircuiTree 20:30–32, 35
3. Arabi F, Gracia A, Deletage JY and Fremont H (2018) "Vibration test and simulation of printed circuit board," 2018 19th International Conference on Thermal, Mechanical and Multi-Physics Simulation and Experiments in Microelectronics and Microsystems (EuroSimE), pp. 1–7
4. Liu F and Meng G (2014)" Random vibration reliability of BGA lead-free solder joint," Microelectronics Reliability, 54(1), 226–232
5. Tang W, Ren J, Feng G and Xu L (2007) "Study on vibration analysis for printed circuit board of an electronic apparatus," 2007 International Conference on Mechatronics and Automation, Harbin pp. 855–860
6. Karras J et al (2017) "Pop-up mars rover with textile-enhanced rigid-flex PCB body," IEEE International Conference on Robotics and Automation (ICRA), pp. 5459–5466
7. Bell J, Redmond L, Carpenter K, de la Croix J-P (2020) Dynamic characterization of a pop-up folding flat explorer robot (PUFFER) for planetary exploration. Topics in Modal Analysis & Testing 8:383–391
8. Robin A, Guglielmo A, Guy R (2010) Accuracy of simplified printed circuit board finite element models. Microelectron Reliab 50:86–97
9. Pitarresi J, Primavera A (1992) Comparison of modeling techniques for the vibration analysis of printed circuit cards. ASME J Electron Packag 114(4):378–383
10. Mayes R, Gomez A (2006) Part 4: what's shakin', dude? Effective use of modal shakers. Exp Tech 30(4):51–61
11. Ashory M (1999) High quality modal testing methods. PhD Thesis, Imperial College of Science, Technology and Medicine, London
12. Rafieian F, Zhaoheng L, Hazel B (2009) Dynamic model and modal testing for vibration analysis of robotic grinding process with a 6DOF flexible-joint manipulator. IEEE International Conference on Mechatronics and Automation (ICMA), Changchun, China
13. Thomas C, Dohrmann C (1998) Support conditions, their effect on measured modal parameters. Proceedings of the 16th International Modal Analysis Conferences, pp 815–828
14. Larsson D (1997) Using modal analysis for estimation of anisotropic material constants. J Eng Mech 123(3):222–229
15. Roettgen D, Allen M (2017) Nonlinear characterization of a bolted, industrial structure using a modal framework. Mech Syst Signal Process 84:152–170
16. Park K, Allen M (2021) Quasi-static modal analysis for reduced order modeling of geometrically nonlinear structures. J Sound Vib 502:116076
17. Mojahed A, Liu Y, Bergman L, Vakakis A (2021) Modal energy exchanges in an impulsively loaded beam with a geometrically nonlinear boundary condition: computation and experiment. Nonlinear Dyn 103(4):3443–3463
18. Kerschen G, Worden K, Vakakis, A & Govinal J (2006) "Past, present, and future of nonlinear system identification in structural dynamics," Mechanical Systems and Signal Processing 20 (3) (2006) 505–592.
19. Richards C, Singh R (2001) Characterization of rubber isolator nonlinearities in the context of single and multi-degree-of-freedom experimental systems. J Sound Vib 247(5):807–834
20. Luongo A, D'Annibale F (2016) Nonlinear hysteretic damping effects on the post-critical behaviour of the visco-elastic Beck's beam. Math Mech Solids 22(6):1347–1365
21. Perez M (2017) "Origami-inspired robot can hitch a ride with a rover," NASA. https://www.nasa.gov/feature/jpl/origami-inspired-robot-can-hitch-a-ride-with-a-rover/
22. Göge D, Fullekrug U and Link M (2004) "A strategy for the identification and characterization of non-linearities within modal survey testing," Proceedings of the 22nd International Modal Analysis Conference, Section 3.4)
23. Vakakis A, Manevitch L, Mikhlin Y, Pilipchuk V, Zevin A (1996) Normal Modes and Localization in Nonlinear Systems. Wiley, New York
24. Feldman M (2011) "Hilbert transform in vibration analysis," Mech. Syst. Signal Process., 25 (3) (Apr. 2011), pp. 735–802
25. Kerschen G, Vakakis A, Lee Y, McFarland D and Bergman L (2008) "Toward a fundamental understanding of the Hilbert-Huang transform in nonlinear structural dynamics," J Vib Control 14(1–2): 77–105.
26. Gottlieb O, Feldman M and Yim S (1996) "Parameter identification of nonlinear ocean mooring systems using the Hilbert transform," Journal of Offshore Mechanics and Arctic Engineering, 118 (1996) 29–36 (Section 3.2)
27. King F (2009) Hilbert transforms: (Encyclopedia of Mathematics and its Applications). Cambridge University Press, Cambridge, p 1440

28. Ondra V, Sever I, Schwingshackl C (2017) A method for detection and characterization of structural non-linearities using the Hilbert transform and neural networks. Mech Syst Signal Process 83:210–227
29. Worden K (2000) Nonlinearity in structural dynamics: the last ten years. Proceedings of the European COST F3 Conference on System Identification and Structural Health Monitoring, Madrid, pp 29–52
30. Ghiringhelli G, Terraneo M (2015) Analytically driven experimental characterization of damping in viscoelastic materials. Aerosp Sci Technol 40:75–85
31. Anastasio D, Marchesiello S, Kerschen G, Noël JP (2019) Experimental identification of distributed nonlinearities in the modal domain. J Sound Vib 458:426–444
32. Caughey T, Vijayaraghavan A (1970) Free and forced oscillations of a dynamic system with "linear hysteretic damping" (non-linear theory). Int J Non-Linear Mech 5(3):533–555
33. Torvik P (2003) "A note on the estimation of nonlinear system damping," J Appl Mech 70
34. Marple L (1999) Computing the discrete-time 'analytic' signal via FFT. IEEE Trans Signal Process 47(9):2600–2603
35. Simon M, Tomlinson GR (1984) Use of the Hilbert transform in modal analysis of linear and non-linear structures. J Sound Vib 96(4):421–436
36. Kragh K, Thomsen D (2010) "Experimental detection and quantification of structural nonlinearity using homogeneity and Hilbert transform methods,", Proceedings of the International Conference on Noise and Vibration Engineering, 3173–3188
37. Wu B (2014) A correction of the half-power bandwidth method for estimating damping. Arch Appl Mech 85:315–320
38. Kammer D, Tinker M (2004) Optimal placement of triaxial accelerometers for modal vibration tests. Mech Syst Signal Process 18(1):29–41
39. Salama M, Rose T and Garba J (1987) "Optimal placement of excitations and sensors for verification of large dynamical systems," 28th Structures, Structural Dynamics and Materials Conference
40. Ewins DJ (2000) Modal testing: Theory and practice. Research Studies Press
41. Yang Q, Lim G, Lin R, Yap F, Pang H and Wang Z (1997) "Experimental modal analysis of PBGA printed circuit board assemblies," Proceedings of the 1997 1st Electronic Packaging Technology Conference (Cat. No.97TH8307)
42. Wolf J and Society of Automotive Engineers (1984) "The influence of mounting stiffness on frequencies measured in a vibration test," International Congress and Exposition